



## NUMERICAL INVESTIGATION OF FLUID ELASTIC STABILITY

### Prof. Dr. Saïd Mounsif

Universidade Federal do Pará, DEM, CT, Campus Universitário do Guama, 66075-900, Belém, PA, Brasil, e-mail: [smounsif@ufpa.br](mailto:smounsif@ufpa.br)

### Prof. Dr. Newton Sure Soeiro

Universidade Federal do Pará, DEM, CT, Campus Universitário do Guama, 66075-900, Belém, PA, Brasil, e-mail: [nsoeiro@ufpa.br](mailto:nsoeiro@ufpa.br)

**Abstract:** *Unsteady flow fields around airfoils pitching or/and plunging are investigated. The objective of this study is to show the influence of the aeroelastic parameters that characterize the airfoils, in an incompressible flow. In the present work, a finite-volume numerical method is used for the solution of the two-dimensional unsteady Navier-Stokes equations in general moving curvilinear coordinates to predict the flow past an airfoil. The method employs the semi-strong conservation form of the governing equations with pressure and physical contravariant velocity components as dependent variables. The SIMPLE algorithm is used to handle the pressure-velocity coupling. The flow field calculation is strongly coupled with the dynamic response of the airfoil, which is modeled as an elastic structure. Different cases in fluid-structure interactions are studied. Firstly, we examine the case where the airfoil has only a single-plunge-degree-of-freedom and we investigate the galloping instability phenomena. Then, the airfoil can just pitch about the mid-cord or the quarter-cord where the steady instability called divergence occurs. Finally, the airfoil motion consists in plunging and pitching. In this case the torsion-plunge coupled instabilities-flutter are simulated. For these fluid elastic instability problems, we show that the results produced by the proposed solution method are in excellent agreement with those predicted numerically as well as with experimental data.*

**Keywords:** *fluid-structure interaction, fluid-elastic instability, and unsteady finite-volume numerical simulation.*

## 1. INTRODUCTION

During the past two decades, considerable research has been conducted into the problem of unsteady aerodynamics of an oscillating airfoil. Most of previous research efforts in this area was directed to unsteady wing loading associated with dynamic stall phenomenon, as reviewed by McCroskey (1988), Carr (1988) and Gad-el-Hak (1987). McCroskey et al (1976) performed extensive experimental investigations of unsteady, two-dimensional subsonic flows over oscillating airfoils.

In these investigations, it has been pointed out that unsteady flowfields around pitching airfoils experiencing the dynamic stall phenomenon are characterized by massive recirculating regions and numerical simulations can only be achieved by solving the Navier-Stokes equations with a turbulence model.

In this study, we investigate the influence of the aeroelastic parameters that characterize the airfoil, in an incompressible flow. A finite volume method is used to solve the Reynolds-Averaged-Navier Stokes equations (RANSE). A second-order accurate three-level fully implicit time scheme is used with the strong coupling between the fluid flow calculation and the dynamic response of the airfoil.

## 2. OUTLINE OF COMPUTATION TECHNIQUE

### 2.1 FLUID FLOW SIMULATION

The unsteady, incompressible motion of viscous fluid is governed by the familiar continuity and the Reynolds averaged Navier-Stokes equations, in conjunction with the isotropic turbulent viscosity hypothesis. The eddy viscosity, which relates the Reynolds stresses to the corresponding mean rates of strain, is calculated using the two-layer k- $\epsilon$  model of Frank et al. (1991). The governing equations in the general moving co-ordinates  $x^{(i)}$ , using physical contra-variant velocity components  $V^{(i)}$ , may be written in the following general tensor form:

$$\frac{\Delta}{\Delta t}(\rho\Psi) + \frac{\Delta}{\Delta x^{(j)}} \left[ \rho\Psi V_r^{(j)} - \Gamma_\Psi g^{(jm)} \frac{\partial\Psi}{\partial x^{(m)}} \right] = S_\Psi \quad (1)$$

Where:  $\Psi$  stands for velocity components, turbulent kinetic energy k, its dissipation, and in the case of the continuity equation, unity.

$\Gamma_\Psi$  is the coefficient of total diffusion, and  $S_\Psi$  is the source term pertaining to particular variables.

$V_r^{(j)}$  is the relative velocity:  $V_r^{(j)} = V^{(j)} - V_g^{(j)}$ , where the grid velocity  $V_g^{(j)}$  satisfy the space conservation law in order to take into account the change in time of the co-ordinate system. Details of the origin and the way of incorporating this additional equation can be found in Mounsif (1992).

The transport equations (1) are discretized by employing the finite volume method and a fully implicit temporal differentiation. The normal derivative diffusion terms are approximated by a central difference scheme with the cross-derivatives being treated as an additional source. For the convective terms, a third-order "QUICK"(Quadratic Upstream Interpolation for Convective Kinematics) scheme is employed. Details of the present fluid flow computation and results are discussed by Mounsif (1992) and Mounsif et al. (1995, 1997).

### 2.2 AEROELASTIC MODEL

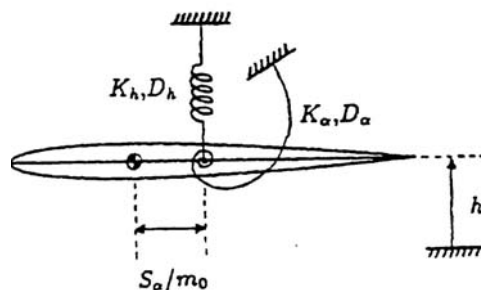


Figure 1. Aeroelastic Structural Model

The dynamic response of the elastic airfoil under the effect of the fluid flow is modeled as an elastic rigid structure using a two-degree-of-freedom spring/mass system Fig. (1). The airfoil can translate or/and rotate (simulation of the bending and twisting of wing). The equations governing this motion (Blevins, 1977) are:

$$m_0\ddot{h} + S_\alpha\ddot{\alpha} + D_h\dot{h} + K_h h = L \quad ; \quad S_\alpha\ddot{h} + I_\alpha\ddot{\alpha} + D_\alpha\dot{\alpha} + K_\alpha(\alpha - \alpha_0) = M \quad (2)$$

Where  $h$  is the vertical displacement,  $\alpha$  is the geometric angle of attack,  $m$  is the airfoil mass per unit span,  $S_\alpha$  is the mass static moment,  $I_\alpha$  is the mass moment of inertia,  $K_h$  and  $K_\alpha$  are the spring stiffness coefficients and  $D_h$  and  $D_\alpha$  are the structural damping coefficients.  $L$  is the net applied aerodynamic force in the vertical direction, while  $M$  is the net applied aerodynamic pitching moment and  $\alpha_0$  is the initial incidence. The natural frequencies in pitch and plunge are  $\omega_\alpha = \sqrt{K_\alpha/I_\alpha}$  and  $\omega_h = \sqrt{K_h/m_0}$ , respectively. The damping factor,  $\zeta = D/D_{crit}$  where  $D_{crit}$  represents the critical damping level and is equal to  $2\sqrt{K_h m_0}$  for the vertical axis and  $2\sqrt{K_\alpha I_\alpha}$  for the pitch axis. The system (2) is transformed to the non-dimensional form:

$$\begin{aligned} \ddot{h} + x_\alpha\ddot{\alpha} + 2\omega_h\zeta_h\dot{h} + \omega_h^2 h &= \frac{2 C_L}{\pi \mu} \\ x_\alpha\ddot{h} + r_\alpha^2\ddot{\alpha} + 2\omega_\alpha r_\alpha^2\dot{\alpha} + \omega_\alpha r_\alpha^2(\alpha - \alpha_0) &= \frac{2 C_M}{\pi \mu} \end{aligned} \quad (4)$$

With:  $x_\alpha = S_\alpha/mc$  and  $r_\alpha^2 = I_\alpha/mc^2$

The system of equations (3) is integrated in time using a fourth-order Runge-Kutta algorithm. The integration takes place immediately after the calculation of aerodynamic coefficients in the main algorithm and proceeds from time  $t$  to  $t + \Delta t$ . The linear and angular accelerations obtained are then returned to provide update values for the aerodynamic calculations.

### 3. NUMERICAL RESULTS

#### 3.1 DYNAMIC-STALL

The NACA0012 airfoil is considered in oscillatory motion at the quarter of chord, and the time dependent angle of attack is defined as:

$$\alpha = \alpha_0 + \Delta\alpha \cos(2kt^*) \quad (5)$$

Where  $k$  is the reduced frequency and  $t^*$  the non-dimensional time  $t^* = tU_\infty/c$ , defined from de chord  $c$  of the airfoil. The reduced frequency represents the ratio of tow time scales: one imposed by the pitching motion  $(2\pi f)^{-1}$  and the other by the free-stream velocity  $c/2U_\infty$ , so  $k = 2\pi f c / 2U_\infty$ . The case considered is a NACA0012 airfoil undergoing oscillatory pitch with the following parameters:  $\alpha_0 = 15^\circ$ ,  $\Delta\alpha = 10^\circ$ ,  $k = 0.15$  and  $R_e = 10^6$ , the Reynolds number, based on the airfoil chord. This case corresponds to the deep-stall case of experimental data of McAlister et al., (1982).

The time history of the lift coefficient is presented in Fig. (2). As it is seen, the details deep-stall hysteresis loops measured in experiments are captured by the present computations. Quantitative differences do exist but are all within the uncertainty bounds of the experimental study.

During the upstroke, the computed lift coefficient increases linearly until the leading-edge vortex forms (see Fig. (3)). The formation of the trailing-edge vortex then causes a steep increase in the lift. At the maximum incidence, the flow field changes rapidly and the dynamic stall vortex separates from the airfoil near the leading. As a result of burst of the bubble at the trailing edge and the shedding of clock-wise vorticity, the lift drops drastically. The overestimation of the lift coefficients due to over-prediction of the trailing-edge vortex suction, in the computations may be attributed to the poor performance of the turbulence model in the wake region.

During the downstroke, following the shedding of the trailing edge vortex, the lift initially decreases rapidly. As the flow reattaches at the trailing edge and as the secondary vortex structures develop, the lift curve flattens. The minimum lift is observed at  $\alpha \approx 10 \text{ deg}$  just before the flow attaches fully on the upper surfaces. In the experiments, reattachment occurs later and the minimum lift is realized at  $\alpha = 7 \text{ deg}$ . The early reattachment of the boundary layers in the computed results as compared to the experimental data, may be attributed to the fully turbulent flow assumption. The development of the leading-edge suction then drives the lift toward the steady – state values. However, the low pressure aft of the midchord on the upper surface delays the recovery process until  $\alpha \approx 5 \text{ deg}$  is reached.

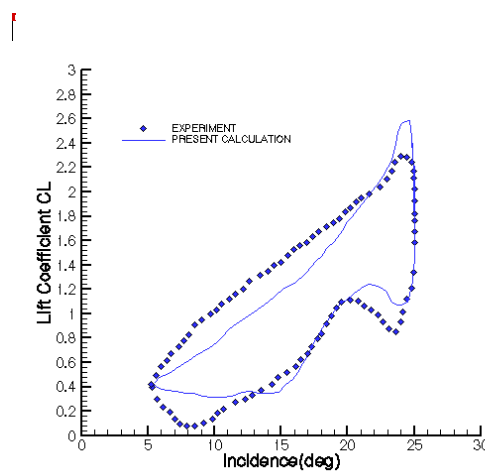
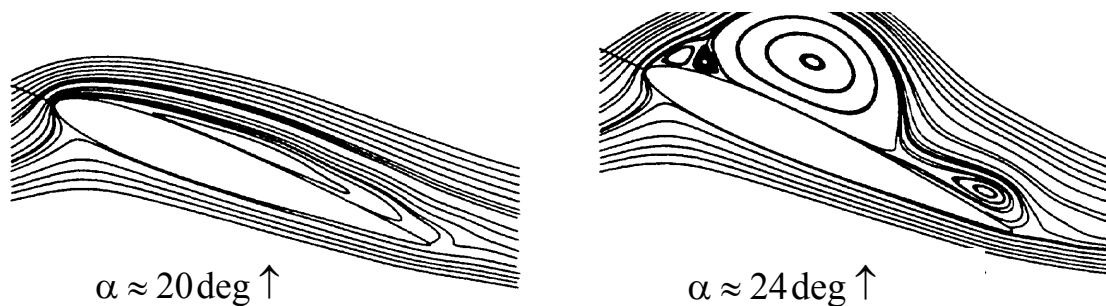


Figure 2. Dynamic stall: Hysteresis loops



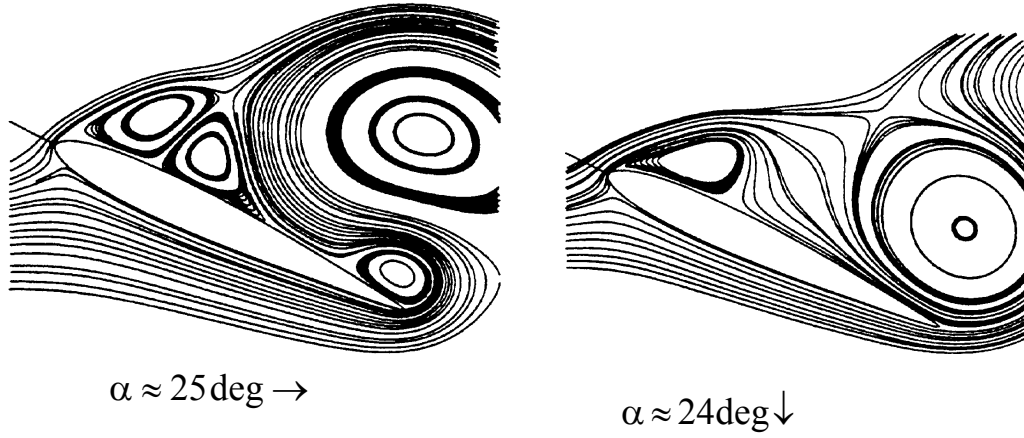


Figure 3. Instantaneous streamlines at Dynamic stall

### 3.2 ELASTIC INSTABILITY RESULTS

Aeroelastic response analyses are carried out for a NACA 0012 airfoil that is considered as a single and low degree of freedom systems. In all cases, the airfoil pitches about mid-chord and the initial incidence is  $\alpha = 0.1 \text{ rad}$ . The Reynolds number, based on the airfoil chord is  $10^6$ . We use a  $100 \times 60$  grid and a time step  $\Delta t = 0.01$ .

#### 3.2.1 PLUNGING ONLY

At  $m_0 = 1.0$ , the dynamic response is unstable even with a damping coefficient  $\zeta = 1.0$  (see Fig. (4.a)). If, instead of a frequency  $\omega_h = \frac{\pi}{2}$ , we use a higher frequency  $\omega_h = 2\pi$ , the responses obtained with or without a damping coefficient are unstable (see Fig. (4.b)). At  $m_0 = 10.0$ : (a higher mass case), the solutions are stable. Figure (5.a) presents the response for a frequency  $\omega_h = \frac{\pi}{2}$ . With or without a damping coefficient, the response is stable and the equilibrium position is  $h = 7.2 \cdot 10^{-3}$ . The aerodynamic coefficients are those of the fixed airfoil. With a frequency  $\omega_h = 2\pi$ , the response is stable with a damping coefficient  $\zeta = 1.0$ . The equilibrium position is  $h = 4.5 \cdot 10^{-4}$  and the aerodynamic coefficients are those of the fixed airfoil. With a zero damping, the solution is oscillating with a period  $T = 1.0$ , Figure (5.b) presents the plunging displacement for the case where the frequency is  $\omega_h = 2\pi$  and the damping coefficient is  $\zeta = 0.0$ . Two time steps are used:  $\Delta t = 0.01$  (solid line) and  $\Delta t = 0.005$  (dashed line). The result is similar with both time steps; a slight difference exists about the first periods

#### 3.2.2 PITCHING ONLY

At  $I_\alpha = 1.0$ : firstly we consider a frequency  $\omega_\alpha = \pi/2$ . With a zero damping coefficient and a mass  $m_0 = 1.0$ , a dynamic response of the airfoil is unstable. A case with a mass  $m_0 = 10.0$  corresponds to the neutrally stable condition (see Fig. (6)). The phase plane plots of the pitching velocity vs. the incidence (see Fig. (7)) and the FTT spectrum (see Fig. (8)), verify that this motion is dominated by a simple harmonic motion with a period  $T = 4.55$ .

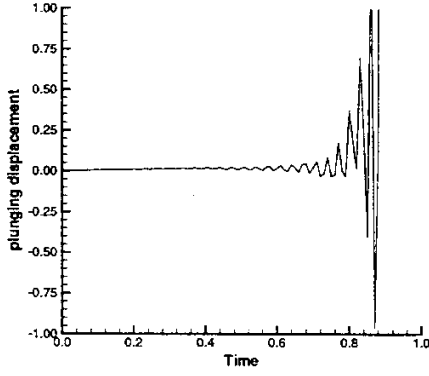


Figure 4a. Plunging displacements

$$m_0 = 1.0, \omega_h = \frac{\pi}{2}, \zeta = 1.0$$

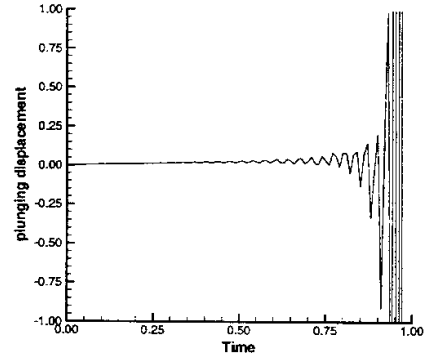


Figure 4b. Plunging displacements

$$m_0 = 1.0, \omega_h = 2\pi, \zeta = 1.0$$

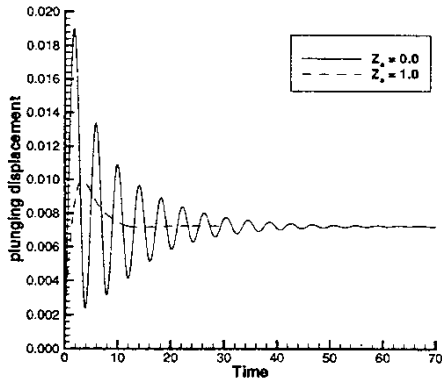


Figure 5a. Plunging displacements:

$$m_0 = 10.0, \omega_h = \frac{\pi}{2}$$

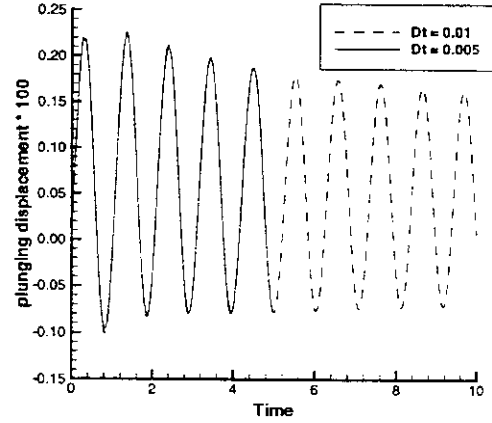


Figure 5b. Plunging displacements

$$m_0 = 10.0, \omega_h = 2\pi, \zeta = 0.0$$

With a damping coefficient  $\zeta_\alpha = 0.5$ , the motion shows a chaotic behavior with a mass  $m_0 = 1.0$ . Then, with a mass  $m_0 = 10.0$ , the motion is stable and we find the aerodynamic coefficients of the fixed airfoil. With a damping coefficient  $\zeta_\alpha = 1.0$ , the motion is periodic (see Fig. (9)), while a mass  $m_0 = 10.0$  corresponds to a stable condition. Then, the frequency  $\omega_\alpha = 2\pi$  is chosen with a mass  $m_0 = 10.0$ . If the damping coefficient is zero, the motion is periodic (see Fig. (10)), and with  $\zeta_\alpha = 0.5$  the motion is stable. With a zero damping coefficient, the incidence variation is weaker than the cases where the frequency is  $\omega_\alpha = 2\pi$ .

At  $I_\alpha = 10.0$ : with a zero damping a mass  $m_0 = 1.0$ , the phase  $\omega_\alpha = \pi/2$  corresponds to the neutrally stable condition (see Fig. (11)). The phase plane plots of the pitching velocity vs. the incidence and the FTT spectrum (see Fig. (12) and Fig. (13)), verify that this motion is dominated by a simple harmonic motion which have a period  $T = 4.55$ . If the mass higher ( $m_0 = 10.0$ ), the motion is neutrally stable and the period is  $T = 1.0$ . For this frequency, the amplitude variation of the pitching oscillation is again weaker than those of case where  $I_\alpha = 1.0$ , and  $m_0 = 10.0$ .

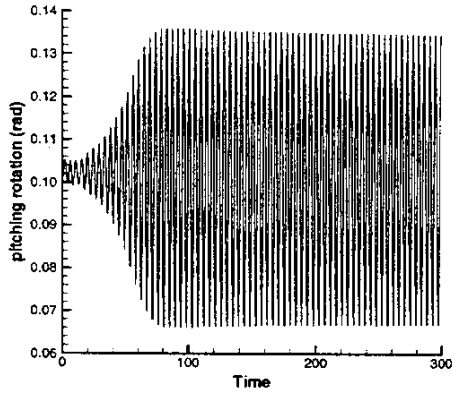


Figure 6. Pitching rotations  $I_\alpha = 1.0$ ,

$$\omega_\alpha = \frac{\pi}{2} \quad m_0 = 10.0 \quad \zeta_\alpha = 0.0$$

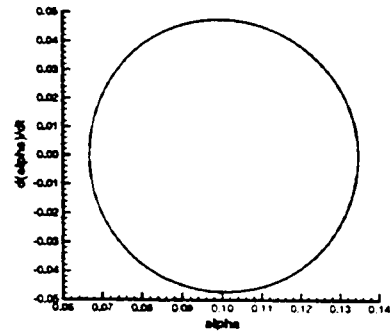


Figure 7. Phase plane plot of the pitching velocity vs. the incidence

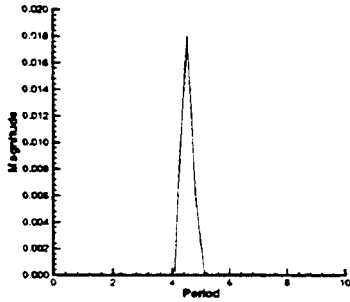


Figure 8. FFT period spectrum of the pitching rotation

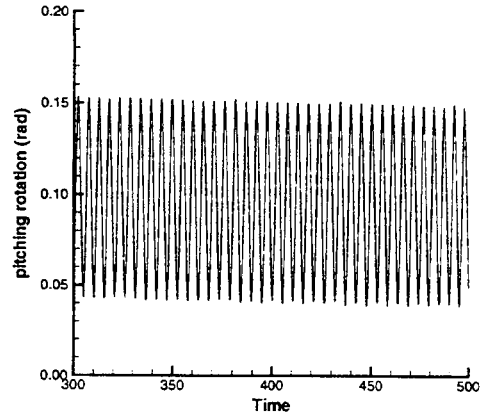


Figure 9. Pitching rotations  $I_\alpha = 1.0$ ,

$$\omega_\alpha = \pi/2 \quad m_0 = 1.0 \quad \zeta_\alpha = 1.0$$

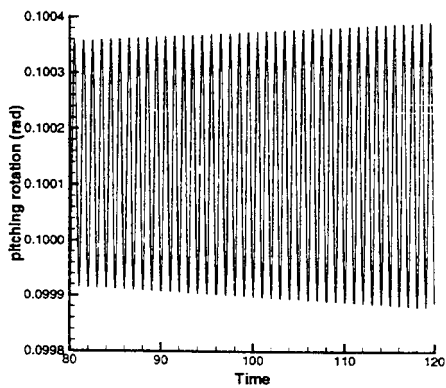


Figure 10. Pitching rotations  $I_\alpha = 1.0$ ,

$$\omega_\alpha = 2\pi \quad m_0 = 1.0 \quad \zeta_\alpha = 0.0$$

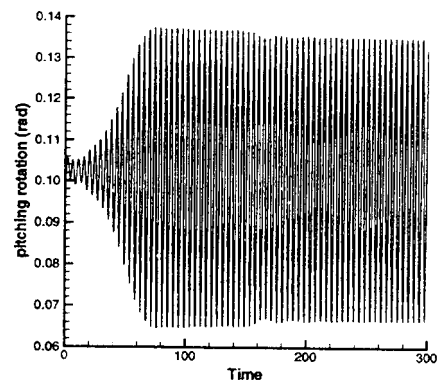


Figure 11. Pitching rotations  $I_\alpha = 10.0$

$$\omega_\alpha = \pi/2 \quad m_0 = 1.0 \quad \zeta_\alpha = 0.0$$

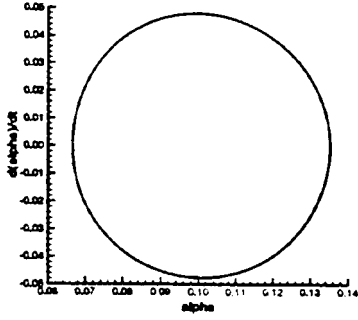


Figure 12. Phase plane plot of the pitching velocity vs. the incidence

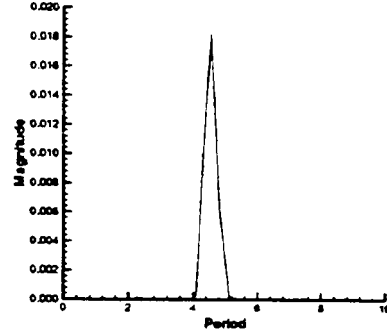


Figure 13. FFT period spectrum of the pitching rotation

### 3.2.3 PLUGING and PITCHING

The motion of the NACA 0012 consists in coupled torsion-plunge vibration about a mid-chord axis. With a single plunging degree-of-freedom, the motion with  $m_0 = 1.0$  is unstable, so only the case  $m_0 = 10.0$  is analyzed.

#### 3.2.3.1 Case 1: $\omega_h = \pi/2$ and $\zeta_h = 0.0$

Firstly, we consider a moment of inertia  $I_\alpha = 1.0$  and a zero damping coefficient. With a pitching frequency  $\omega_\alpha = \frac{\pi}{2}$ , the dynamic response until  $t^* = 200$  presents beatings that disappear when the plunging displacement and the pitching incidence grow (see Fig. (14)). If the pitching frequency is higher ( $\omega_\alpha = 2\pi$ ), the response for plunging displacement tends towards a fixed position  $h = 7.2 \cdot 10^{-3}$ , while the response of the pitching rotation is oscillating with a period  $T = 1.0$  (see Fig. (15)). Secondly, we consider a moment of inertia  $I_\alpha = 10.0$  and a pitching frequency  $\omega_\alpha = \pi/2$ . With a zero pitching damping coefficient, the dynamic response of the plunging and the pitching incidence are unstable (see Fig. (16)). The magnitudes of oscillations are weaker than the case where  $I_\alpha = 1.0$ .

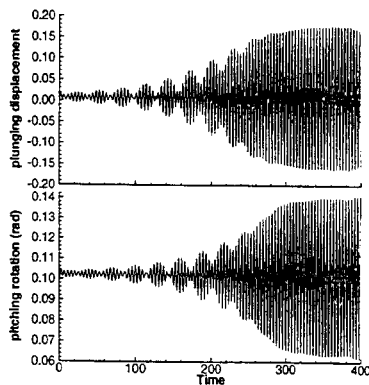


Figure 14. Plunging-Pitching  $m_0 = 10.0$ ,  
 $I_\alpha = 1.0$ ,  $\omega_\alpha = \omega_h = \pi/2$

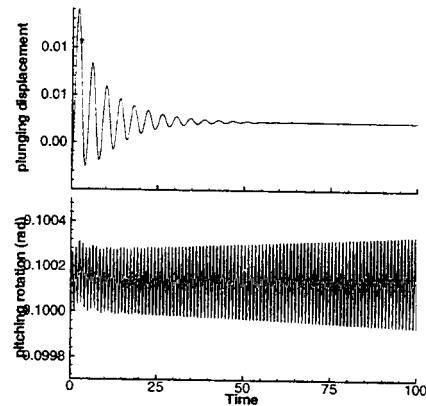


Figure 15. Plunging-Pitching  
 $m_0 = 10.0$ ,  $I_\alpha = 1.0$ ,  $\omega_\alpha = \omega_h = 2\pi$

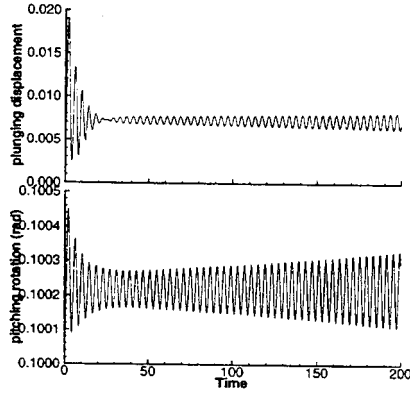


Figure 16. Plunging-Pitching  $m_0 = 10.0$ ,  
 $I_\alpha = 10.0$ ,  $\omega_\alpha = 2\pi$ ,  $\omega_h = \pi/2$

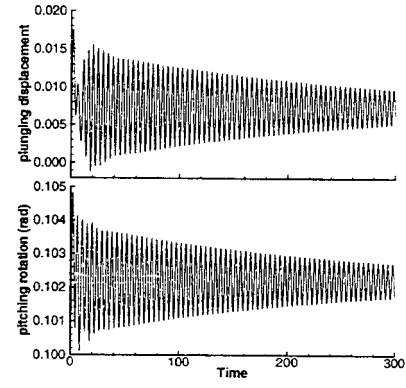


Figure 17. Plunging-Pitching  $m_0 = 10.0$ ,  
 $I_\alpha = 1.0$ ,  $\omega_\alpha = \omega_h = \pi/2$ ,  $\zeta_h = 0.1$ ,  $\zeta_\alpha = 0.0$

### 3.2.3.2 Case 2: $\omega_h = \pi/2$ and $\zeta_h = 0.1$

For this case, we choose a moment of inertia  $I_\alpha = 1.0$ , a pitching frequency  $\omega_\alpha = \pi/2$  and a zero pitching damping coefficient. Dynamic responses of the plunging and the pitching rotation are oscillating (see Fig. (17)).

We don't have the beating phenomenon that is present when the plunging damping coefficient is zero. The period of the plunging displacement and the pitching incidence is identical,  $T = 4.55$ .

### 3.2.3.3 Case 3: $\omega_h = 2\pi$ and $\zeta_h = 0.0$

We consider a moment of inertia  $I_\alpha = 1.0$  and a pitching frequency  $\omega_\alpha = \pi/2$ . A zero pitching damping coefficient corresponds to a neutrally stable condition (see Fig. (18)).

The magnitude of the incidence is similar to those where the plunging frequency is  $\omega_h = \pi/2$ , but the magnitude of the plunging displacement is weaker. If the pitching damping coefficient is  $\zeta_\alpha = 0.1$ , the dynamic responses are no more neutrally stable (see Fig. (19)).

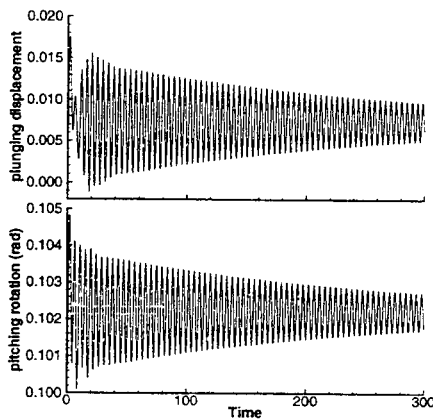


Figure 18. Plunging-Pitching  $m_0 = 10.0$ ,  
 $I_\alpha = 1.0$ ,  $\omega_\alpha = \omega_h = \pi/2$

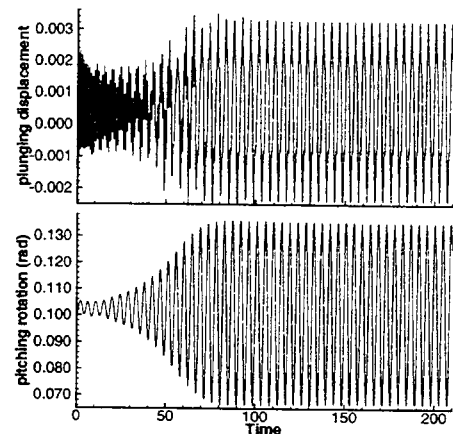


Figure 19. Plunging-Pitching  $m_0 = 10.0$ ,  
 $I_\alpha = 1.0$ ,  $\omega_h = 2\pi$ ,  $\omega_\alpha = \pi/2$

#### 4. CONCLUDING REMARKS

The unsteady flowfields around large amplitude oscillating airfoils have been simulated numerically with the intention to evaluate the ability of our computational code to predict unsteady flows with fluid-structure interactions. The computed unsteady flowfields and aerodynamic loads for the case presented in this paper agreed well with the experimental data. Massive recirculating regions, the formation and convection of large vortex structures, and details of the dynamics stall phenomenon have been identified. The full viscous flow analysis of the NACA 0012 airfoil has shown that the dynamics of the leading-edge vortex has a dominant effect on the dynamic stall behavior. The response results obtained for a single degree of freedom system of plunging for an airfoil with  $m_0 = 1.0$  are unstable. With a mass  $m_0 = 10.0$ , we don't find neutrally stable conditions but only stable solutions. When the airfoil pitches about the mid-chord, the response results obtained are often neutrally stable. In this case, the motion is dominated by a single harmonic motion. When the airfoil plunges and pitches about the mid-chord, the pitching motion is dominated by a single harmonic motion while the plunging motion is a single non-harmonic motion.

#### 4. REFERENCES

- Blevins, R., 1977, "Flow induced Vibrations. Van Nostrand Reinhold Company, New York.
- Carr, L.W., 1988, "Progress in Analysis and Prediction of Dynamic Stall", Journal of Aircraft, Vol. 25, pp. 6-17.
- Frank R. and Rodi W., "Calculation of vortex shedding past a square cylinder with various turbulence models. Eight Symposium on Turbulent Shear Flows", Technical University of Munich, pp. 9-21.
- Gad-el-Hak, M., 1987, "Unsteady Separation on Lifting Surfaces," Applied Mechanics Review," Vol. 40, pp. 441-453.
- McAlister, K., Pucci, S., McCroskey, W., and Carr, L., 1982, "An experimental Study of Dynamic Stall on Advanced Airfoil Sections, Pressure and Force Data", NASA TM 84245.
- McCroskey, W.J., 1988, "Some Current Research in Unsteady Fluid dynamics", The 1976 Freeman Scholar Lecture, ASME Transactions Journal of Fluids Engineering, Vol. 99, pp. 8-39.
- McCroskey, W.J., Carr, L.W, and McAlister, K.W., 1976, "Dynamic Stall Experiments on Oscillating Airfoils," AIAA Journal, Vol. 14, pp. 57-63.
- Mounsif, S., 1992, "Modélisation d'Écoulements Instationnaires Autour de Géométries Mobiles, Application aux Interactions Fluid-Structures", Thèse de Doctorat, Institut National Polytechnique de Grenoble, INPG, Grenoble, France.
- Mounsif, S. and Amarante, A., L., M., 1995, "A numerical Model for the Fluid-Structure Interaction. Analysis of Flow past a Two-dimensional Body", The 3rd Workshop AIAA, IAHR, Turbinas Hidraulicas e Hidrodinamicas, Mendoza. Vol. 2, pp. 23-32.
- Mounsif, S. and Amarante, A., L., M., 1997, "A Finite Volume Method for the Computation of Fluid Flow with Moving Grid For Fluid-Structure Interactions", The 4<sup>th</sup> International Symposium on Fluid-Structure Interactions, Aeroelasticity, Flow-Induced Vibration and Noise, Dallas, ASME 1997, AD-Vol, 53-1, Vol. 1., pp. 57-65.